Ab Initio Molecular Dynamics Simulation of a Medium-Sized Water Cluster Anion: From an Interior to a Surface-Located Excess Electron via a Delocalized State

Tomaso Frigato,[†] **Joost VandeVondele,**[‡] **Burkhard Schmidt,**[†] **Christof Schütte,**[†] **and Pavel Jungwirth***[,§]

Institut für Mathematik, Freie Universität Berlin, Arnimallee 6, D-14195, Berlin, Germany, Physical Chemistry Institute, Zürich University, Winterthurerstrasse 190, CH-8057 Zürich, Switzerland, and Institute of Organic Chemistry and Biochemistry, Academy of Sciences of the Czech Republic and Center for Biomolecules and Complex Molecular Systems, Flemingovo nam. 2, 16610 Prague 6, Czech Republic

Received: December 7, 2007; Revised Manuscript Received: April 17, 2008

We present a computational study of the structure and dynamics of an excess electron in a medium-sized water cluster aimed at addressing the question of interior vs exterior solvation. Ab initio Born−Oppenheimer molecular dynamics simulations were performed within the DFT framework, employing a hybrid Gaussian and plane-wave formalism together with the PBE exchange-correlation functional and norm-conserving pseudopotentials. Analysis of a 15-ps trajectory allowed us to reach the following conclusions: (i) the excess electron is predominantly located at the cluster surface (even if it is initially placed in the interior), (ii) the computed electron binding energies correlate with the electron localization rather than with its bulk vs surface location, and (iii) a dynamical interconversion between two different H-bond patterns around the electron occurs. The computed electron binding energies and the most relevant features of the IR spectrum are in a very good agreement with results of previous experimental studies.

Introduction

Excess electrons in water, denoted as hydrated electrons, e_{aq}^-, are of fundamental importance in several fields including radiation and atmospheric chemistry, biology, and astrophysics[1–3] and have, therefore, been the subject of significant interest since their discovery in 1962.[4] The ability to bind an electron is a collective property of water molecules: whereas a single water molecule does not bind an excess electron, a water dimer already does.[5] However, the character of the excess electron in a water dimer and in small water clusters in general is different from that in the bulk. In small clusters, the excess electron, commonly denoted as a dipole-bound electron, is weakly bound at the exterior by electrostatic and dispersion interactions.[6–13] Its binding energy is in the 100 meV range, and a relevant fraction of its wave function typically exceeds the size of the water cluster. In contrast, in larger clusters with tens to hundreds of water molecules, the electron binding is stronger (in the electronvolt range) and mainly of electrostatic nature,[14–20] and its properties such as binding energy and solvation structure converge to those observed for hydrated electrons in extended aqueous systems.

Small anionic water clusters offer an appealing alternative to bulk systems, as experiments can be carried out under well-controlled conditions and simulations can be performed with a sufficiently accurate methodology. Bulk properties can be extrapolated from the behavior of clusters of increasing size. However, we stress an important issue concerning the extrapolation of cluster properties to the bulk liquid, namely, temperature. Cluster experiments are typically carried out under cryogenic conditions, so the systems are either nanocrystals or amorphous. Consequently, one should be cautious when extrapolating to the situation of an electron in the bulk liquid.

Despite numerous efforts, electron solvation in water clusters is still not completely understood. One of the most fundamental questions, whether the electron prefers interior solvation or surface solvation, is still a matter of controversy. Surface states were first identified by path integral molecular dynamics (MD) simulations,[21] where they were found to be preferred for clusters comprising 8−32 water molecules. For $(H_2O)_n^-$ with $n \geq 64$, it was deduced that internal solvation becomes energetically favored, implying a surface-to-bulk transition in the range $32 \leq n \leq 64$ molecules. Electron photodetachment experiments for clusters up to $n = 69$ showed that the electron binding energy scales linearly with $n^{-1/3}$ for $n \geq 11$.[14] This result is compatible with internally solvated electrons, as a simple theoretical model predicts the same scaling for a spherical charge distribution in a uniform dielectric medium.[21]

An important experimental breakthrough was achieved recently.[15] Monitoring electron photodetachment spectra of small clusters under different experimental conditions, typically at temperatures of around 200 K where such clusters are believed to still be liquid-like, it was possible to demonstrate the copresence of (at least) three different isomers. These isomers were characterized by different values of the electron vertical detachment energy (VDE), and on the basis of VDE scaling arguments and comparison with theoretical calculations, the most stable isomer was described as a bulk state, and the remaining two isomers were identified as surface states. Moreover, it was suggested that the expected surface-to-bulk solvation transition takes place already for rather small clusters ($n \geq 11$). These claims, although supported by later experimental work,[16] have been challenged by quantum-classical pseudopotential simulations,[17] in which the most stable state appears to be a surface state and the surface-to-bulk transition takes place

---

* To whom correspondence should be addressed. E-mail: pavel.jungwirth@uochb.cas.cz.

[†] Freie Universität Berlin.

[‡] Zürich University.

[§] Academy of Sciences of the Czech Republic and Center for Biomolecules and Complex Molecular Systems.

10.1021/jp711545s CCC: $40.75

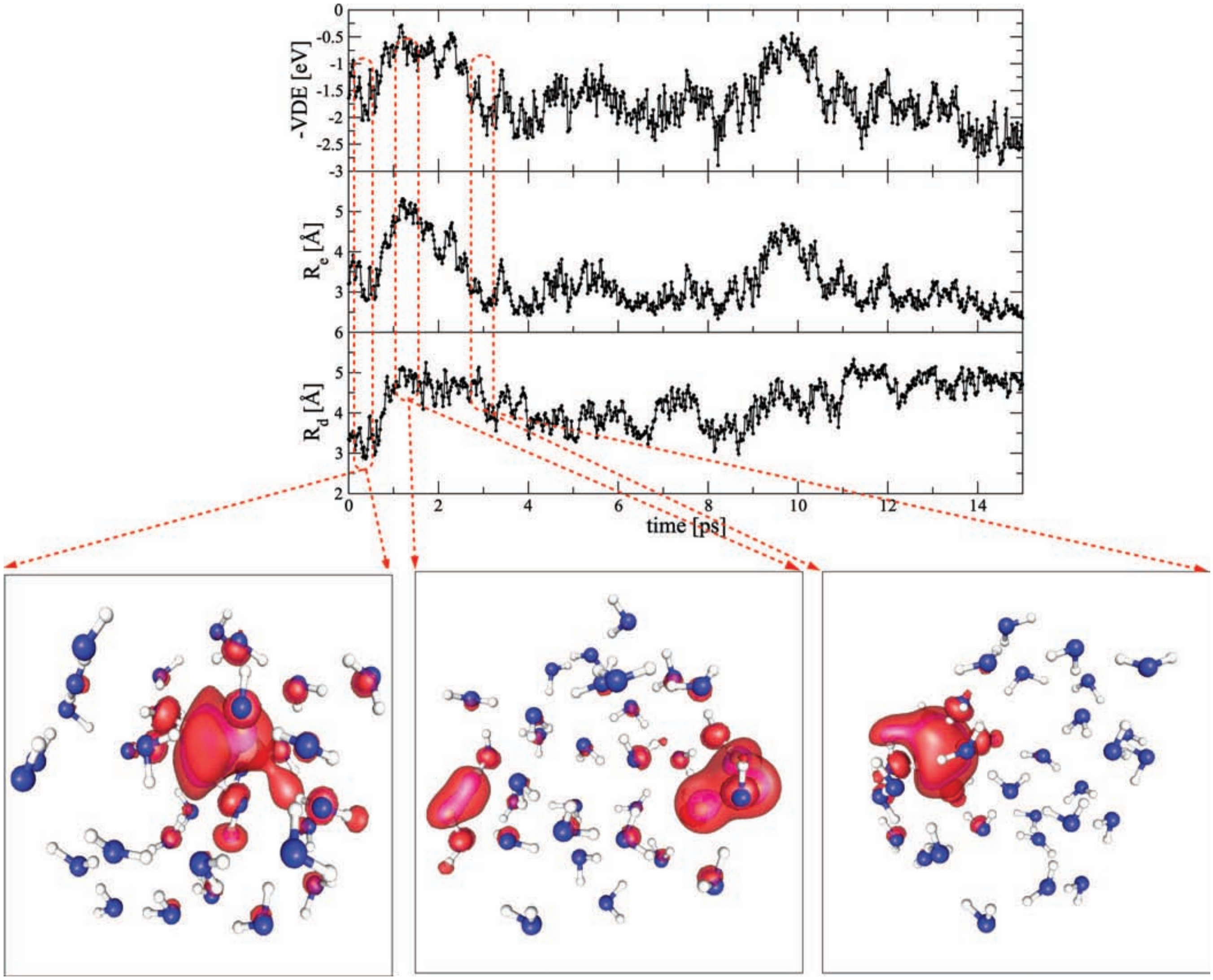

Figure 1. (Top panel) Electron vertical detachment energies (VDEs). (Middle panel) Electron radius of gyration, R_e. (Bottom panel) Mean distance between the excess electron center and the cluster geometrical center, R_d. All data were computed at the PBE-GTH-m-TZV2P level. Below the graphs, the spin density isosurfaces (orange = 0.003, magenta = 0.002, red = 0.001) are shown at t = 0.16, 1.5, and 3 ps from left to right.

for larger clusters. The authors of this computational study also referred to a different theoretical model that gives rise to a $n^{-1/3}$ scaling of VDEs for surface states as well.[22] However, recent high-level ab initio minimizations[19] found internally solvated electrons for water clusters with only 15 H_2O molecules (albeit for high-energy isomers), so the question of internal vs surface electron solvation in water clusters is not yet fully resolved.

Regarding the solvation structure, particular attention has been paid to the local hydrogen-bonding motif around the excess electron. Especially in smaller clusters, deviations from the bulk solvation structure, where the electron is found inside a cavity surrounded by roughly six water molecules,[23] can be expected. A red-shifted HOH bending band was observed experimentally for clusters of up to ~20 water molecules.[10] Ab initio calculations, which confirmed the experimental findings,[9] indicated that this red shift derives from a strong charge transfer to the O−H σ^* orbital of a single water molecule. Both of the hydrogen atoms of this water molecule point toward the electronic cloud in the so-called double hydrogen-bond acceptor (AA) configuration. Vibrational spectra of cryogenic water clusters with 15−50 molecules[20] show that this motif is clearly observed for the smaller clusters, whereas the spectroscopic signature broadens with increasing cluster size, indicating a more delocalized electron binding structure. Such results give rise to an interesting question about the presence and relative stabilities of cavity and single-acceptor molecule structures.

Most previous dynamical simulations of hydrated electrons were performed using a pseudopotential approach. In this approach, only the excess electron is treated as a quantum-mechanical particle, whereas the interactions between the classical water molecules and the excess electrons are described with an empirical pseudopotential.[13,17,18,21,24–28] By construction, such models do not include many-electron effects, except for the recent Drude model study of water hexamer anion.[13] Exceptions to pseudopotential simulations are three studies of a bulk hydrated electron, two based on the Car−Parrinello MD method[29,30] and one employing a quantum-mechanics/molecular-mechanics (QM/MM) approach,[31] and a Car−Parrinello MD study of a surface-trapped electron on ice.[32] It is worth mentioning that the authors of ref 31 explicitly stated that many-electron effects must be taken into account to reproduce the charge transfer to the 2p orbitals of the oxygen atoms surrounding the electron, which is necessary to explain magnetic resonance results.[33] However, to the best of our knowledge, all-(valence-) electron models have been considered only in simulations of either a bulk hydrated electron[29–32] or extremely

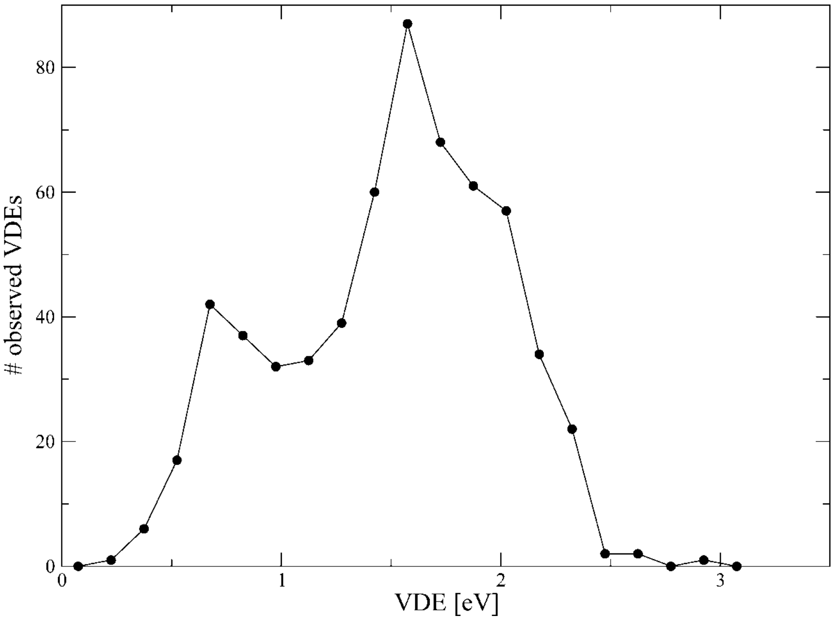

Figure 2. VDE spectrum, computed from the time series shown in Figure 1.

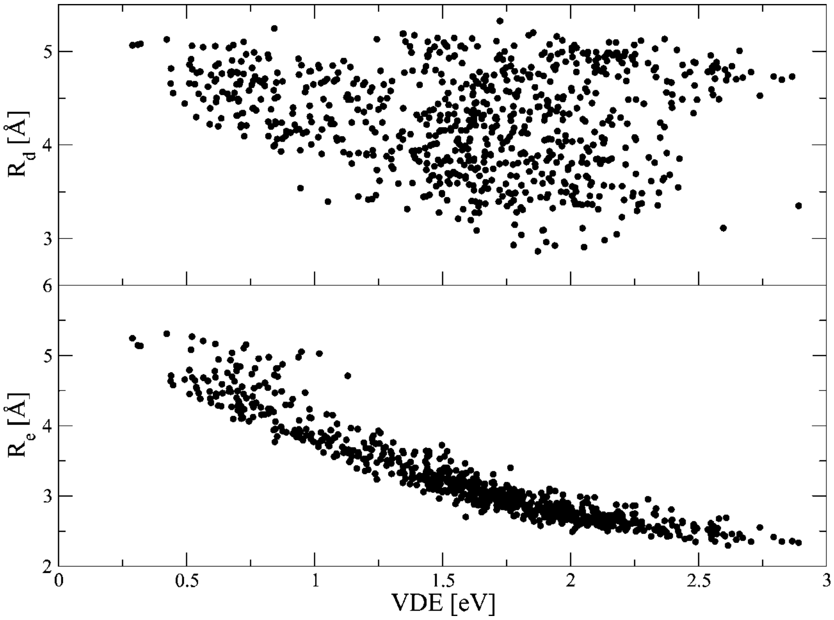

Figure 3. Correlations between VDE and (top) electron position R_d and (bottom) electron radius of gyration R_e.

small clusters [such as $(H_2O)_4^{-}$ [34]], but not medium-sized clusters, for which only one-electron models have been used.[17,18,21]

The present study aims at filling this gap, providing all-(valence-) electron simulations of an excess electron in/on the medium-sized anionic water cluster $(H_2O)_{32}^{-}$. In particular, we aim at providing answers to the following questions: (i) Does the excess electron prefer surface or interior configurations in medium-sized liquid-like water clusters? (ii) How does the electron binding energy correlate with the electron delocalization and location in the cluster, and how do the calculated values relate to those from photoelectron spectroscopy? (iii) How do water molecules arrange around the excess electron, and is the AA motif, found in cryogenic clusters, preserved in the liquid phase? (iv) What are the signatures of electron binding in the vibrational spectrum of the cluster? (v) How accurately does the density functional theory (DFT) employed in the simulations [i.e., the Perdew−Burke−Ernzerhof (PBE) functional] describe the structure and dynamics of the hydrated electron?

At ambient conditions, the chosen intermediate cluster size ensures that the system is small enough that the ab initio simulations are sufficiently efficient to allow for reasonable statistics, whereas the cluster is still large enough to make internal electron solvation principally possible. Even smaller clusters have been shown to be able to accommodate an internally located electron;[19] however, a larger cluster was chosen here for two reasons: First, the electron binding energy is closer to the bulk value. Second, the dispersion interaction (not taken into account at the DFT level used throughout the simulations), the relative contribution of which decreases with cluster size, is less important for the present system than for small clusters.

Methods

Ab initio molecular dynamics simulations were performed using the open source computer code CP2K.[35] In its electronic

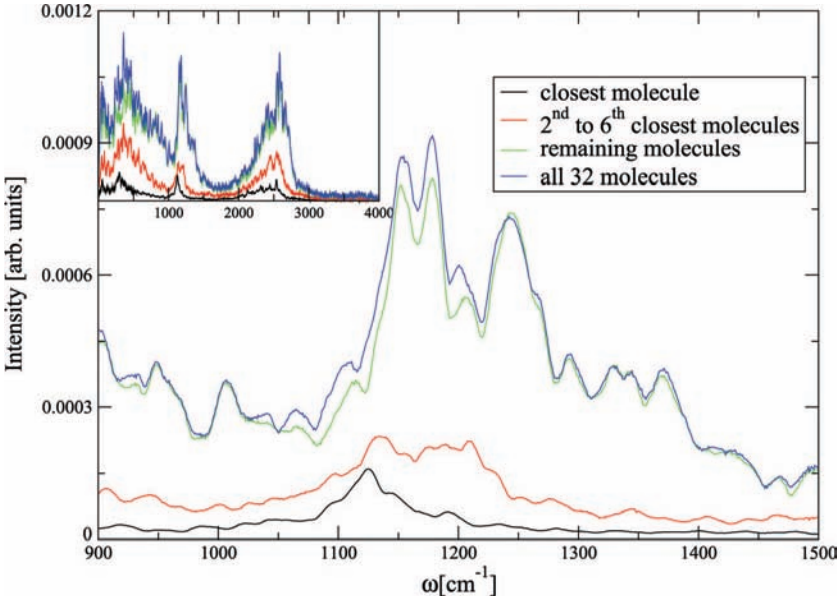

Figure 4. Bending region of the $(H_2O)_{32}^-$ IR spectrum, computed as the Fourier transform of the velocity autocorrelation function extracted from the MD trajectory. Inset: Complete IR spectrum. Three IR spectra were added, obtained from velocities of the water molecule closest to e_{aq}^-, velocities of the second- to sixth-closest molecules, and velocities from the remaining 26 molecules.

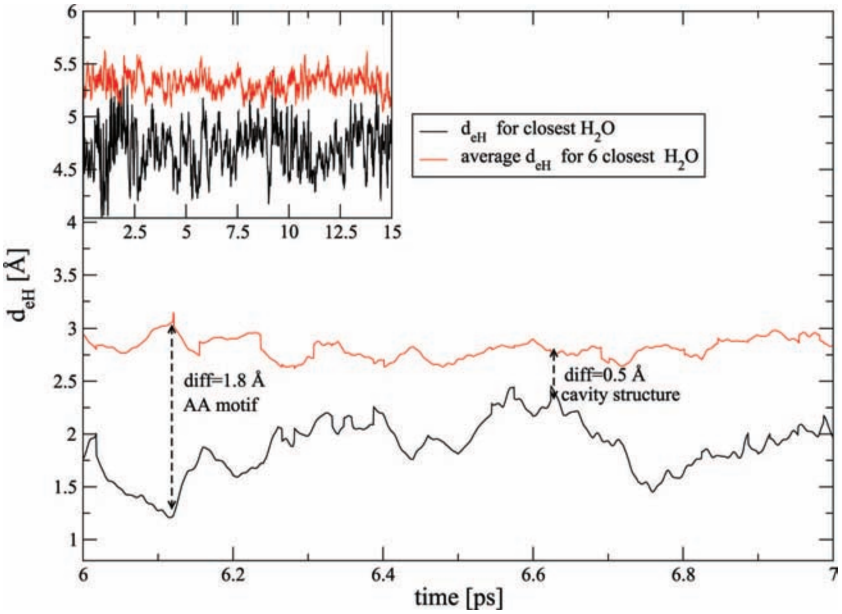

Figure 5. Average $e_{aq}^- \cdots H$ distance for the molecule closest to e_{aq}^- and the six closest molecules to e_{aq}^-. Inset: Complete time series.

structure module, calculations are performed at the DFT level within the hybrid Gaussian and plane-wave method GPW,[36] and the electronic ground-state density is converged at each step (so-called Born−Oppenheimer dynamics). Kohn−Sham orbitals are expanded into atom-centered Gaussian-type orbital functions, and the electron density is represented with an auxiliary plane-wave basis.

A simulation setup very similar to that previously applied successfully to liquid water simulations was chosen.[36,37] Core electrons were removed by the introduction of norm-conserving pseudopotentials developed by Goedecker, Teter, and Hutter (GTH[38]), and a charge density cutoff of 280 Ry was used for the auxiliary basis set. The Perdew−Burke−Ernzerhof (PBE) exchange-correlation functional was used,[39] as it yields liquid water behavior similar to that obtained with the more often employed BLYP functional,[40] but with a lower vapor pressure and consequently more stable clusters.[41] Kohn−Sham orbitals were expanded into a triple-ζ valence basis, with the addition of very diffuse functions, which are particularly important for the proper description of configurations in which the electron is localized on the cluster surface. This basis set, denoted as m-TZV2P, in described in detail in ref 42.

As plane waves are intrinsically periodic, simulations of isolated systems are possible only with the introduction of a cluster correction term[43] and a unit cell at least twice as large as the simulated system (including the electronic density). Therefore, the water cluster was placed in the middle of a cubic box with a length of 20 Å. The system was coupled via a Nosé−Hoover thermostat to a bath at $T = 350$ K to enhance sampling and ensure liquid behavior.[37,40,44] Deuterated water was used, and the equations of motion were integrated with a 0.5 fs time step.

To estimate the accuracy of the electronic structure calculations performed during the Born−Oppenheimer MD run, higher-

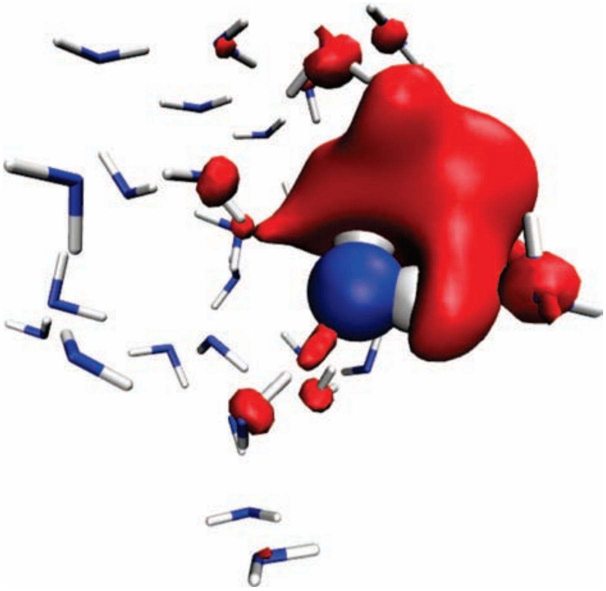

Figure 6. Total spin density (isovalue = 0.001) at $t = 6.12$ ps. The single water molecule with both H atoms pointing toward the electronic density, typical of the AA motif, is drawn with spherical atoms, whereas the other molecules are depicted with a stick model.

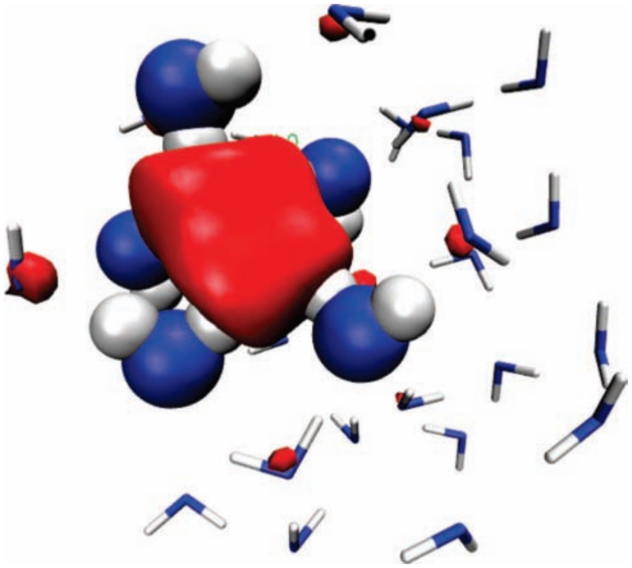

Figure 7. Total spin density (isovalue = 0.001) at $t = 6.62$ ps. The molecules closest to e_{aq}^- are drawn with spherical atoms, whereas the other molecules are depicted with a stick model.

level calculations were performed on a small subset of configurations extracted from the simulated trajectory. First, the effect of the spurious self-interaction energy present in DFT calculations was investigated. It is known that, in systems with unpaired electrons, the self-interaction error present in DFT calculations can lead to inaccurate results.[32,45] However, it has been shown previously that, for a bulk hydrated electron, this does not seem to be the case, and inclusion of self-interaction correction (SIC) terms does not significantly modify the results.[30] A similar behavior was, therefore, expected in our calculations; nevertheless, we checked for the possible effects of self-interaction. The SIC term used was taken from ref 46: $E_{\mathrm{sic}} = -aE_{\mathrm{H}}[m] - bE_{\mathrm{XC}}[m, 0]$, where m is the system total spin density, $E_{\mathrm{H}}[m]$ is the Hartree functional, and $E_{\mathrm{XC}}[m, 0]$ is the exchange-correlation functional. For the parameters of this empirical correction, we followed ref 46 and set $a = 0.2$ and $b = 0$.

Next, the accuracy of the PBE functional used was checked by comparing energies and spin densities extracted from the simulations for representative cluster geometries along the MD trajectory with those calculated at the B3LYP/6-31++G**[47–49] and RIMP2/aug-cc-pVDZ[50–52] levels. As shown in ref 53, with the use of sufficiently diffuse functions, MP2 calculations reach 0.05 eV accuracy for small ($n \leq 4$) electron−water clusters when compared with experimental and coupled-cluster theory results, thus representing quite a reliable benchmark.

In addition to the CP2K program, Gaussian 03[54] and Turbomole[55] V5.9 were used for ab initio single-point energy calculations, and NWChem[56] was used for the classical molecular dynamics equilibration described in the next section. Electronic densities were plotted using the programs VMD[57] and gOpenMol.[58,59]

Results

Initial Conditions. An initial configuration was built with the electron localized in the cluster interior using the following procedure: First, a system consisting of 32 water molecules and an auxiliary iodide anion was considered. A 500-ps classical molecular dynamics equilibration was performed using the AMBER empirical force field,[60] in which the I^- van der Waals radius (2.35 Å) was close to the equilibrium value of the bulk hydrated electron radius (2.5−2.6 Å[31,61,62]). We can thus assume that the water structure around I^- will be similar to that around e^-. The system was coupled to a bath at $T = 250$ K (the relatively low temperature allowed the evaporation of water molecules to be prevented while still keeping the system liquid-like), and a 1-fs time step was used for the integration of the equations of motion. The use of a nonpolarizable empirical potential and short equilibration time resulted in I^- remaining located mainly in the cluster interior.[63] A second stage of equilibration was found to be necessary to avoid spurious effects due to the abrupt switch between an empirical force field and ab initio dynamics. Therefore, a configuration characterized by I^- located inside the water cluster was extracted from the last 10 ps of the equilibration simulation and used as starting configuration for a short (2-ps) ab initio simulation at 350 K. This short simulation was performed with a basis set that did not include extra diffuse functions to prevent the iodide ion from migrating toward the cluster surface.

Once this equilibration procedure was completed, I^- resided in an internal cluster cavity suitable for accommodating an excess electron, with respect to the cavity size and the orientation of surrounding water molecules. The auxiliary iodide anion was then removed and replaced by an electron by simply setting the charge of the water cluster to −1 e. A final production run of 15 ps at 350 K was subsequently performed with the m-TZV2P basis set (i.e., with the very diffuse functions).

Bulk versus Surface Solvation. Three principle observables were monitored during the 15-ps production run at regular 20-fs intervals: (1) the system VDE (which is the vertical binding energy of the excess electron, except for the sign), computed as

$$\mathrm{VDE} = E[(\mathrm{H_2O})_{32}] - E[(\mathrm{H_2O})_{32}{}^-]$$

with both energies evaluated at the anionic geometry; (2) the degree of localization of the excess electron, expressed as its radius of gyration

$$R_e = \sqrt{\frac{\int \rho(x)(x - x_{el})^2 \, dx}{\int \rho(x) \, dx}}$$

where $\rho(x)$ is the excess electron density with its center of mass at

$$x_{el} = \frac{\int \rho(x) x \, dx}{\int \rho(x) \, dx}$$

and (3) as a measure of the distance between the cluster geometrical center, x_{aq}, and the excess electron, the quantity

$$R_d = \frac{\int \rho(x)(|x - x_{aq}|) \, dx}{\int \rho(x) \, dx}$$

The choice of considering the system spin density instead of the highest occupied molecular orbital (HOMO) to represent the excess electron was determined by the fact that the spin density is a measurable quantity, in contrast to molecular orbitals. Moreover, Kohn−Sham orbitals do not have a direct correspondence with molecular orbitals. We verified that the spin density in the electron−water cluster overlapped very well with the differential electronic density (i.e., the difference between electron densities of the anionic and neutral systems in the anionic geometry), although the latter was somewhat more diffuse. Therefore, in the following, we refer to the spin density as the excess electron density.

The three computed quantities along the MD trajectory are shown in Figure 1. Because the cluster was prepared with an interior cavity, e_{aq}^- is first localized inside the water cluster, as can be deduced from the excess electron density plot and the smaller value of R_d. After about 0.5 ps, electron delocalization starts, and a maximum R_e value of about 5 Å is reached after ∼1.5 ps. As can be seen from the spin density isosurface in Figure 1, the electron is now mainly localized at two opposite sides of the cluster, with smaller values of the spin density observed all over the cluster. Finally, the electron radius starts to shrink again. At the end of the localization process ($t \approx 3$ ps), the electron is found at the cluster surface (with R_d displaying higher values compared to the beginning of the simulation). This surface state appears to be relatively stable for 6 ps. Then, a brief delocalization phase is observed, followed again by electron localization on the cluster surface. Note that, during the delocalization phases, the electron remains predominantly at the cluster surface with the two main density lobes located at opposite sides of the cluster.

It is instructive to evaluate the average electron radius of gyration, R_{av}. When the whole trajectory is considered, we obtain R_{av} = 3.24 Å, whereas R_{av} = 2.90 Å when we remove the trajectory segments with a very delocalized electron (0 ps < t < 3 ps and 9 ps < t < 11 ps). Note that the latter value is only about 10% larger than the radius of gyration of a bulk solvated electron.

A quantitive criterion for distinguishing between internal and external states was introduced in ref 17: The electron is considered to be internally solvated when the distance between its center and the cluster center plus its radius, R_e, is smaller than the cluster radius R_{cl}, that is, $|x_{el} - x_{aq}| + R_e < R_{cl}$. According to this criterion, internally solvated electrons are found in less than 3% of snapshots from the present trajectory, all of which belong either to the initial phase of the simulation or to the two delocalization events. For the remaining 97% of the trajectory, the excess electron is localized at the surface of the cluster.

The distribution of VDE values for the whole trajectory is depicted in Figure 2. It is rather broad, exhibiting a major peak at 1.6 eV (about one-half the value of excess electron binding in bulk water) and a side peak at around 0.7 eV. Larger VDEs are related to more localized states, and smaller ones are related to more delocalized configurations of the excess electron. The VDE values thus closely correlate with the degree of electron localization rather than with the electron position within the cluster (see Figure 3).

Solvation Structure and IR Spectrum. The IR vibrational spectrum was estimated as the Fourier transform of the velocity−velocity autocorrelation function, restricted only to the

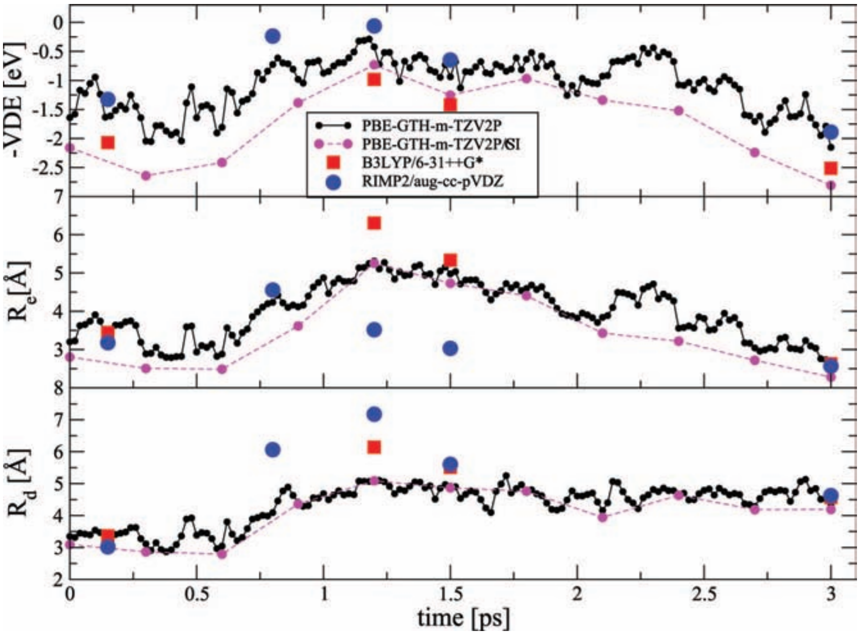

Figure 8. (Top to bottom) VDEs, electron radius of gyration R_e, and mean distance between the excess electron center and the cluster geometrical center R_d. Quantities were computed at different levels of theory, as indicated in the legend.

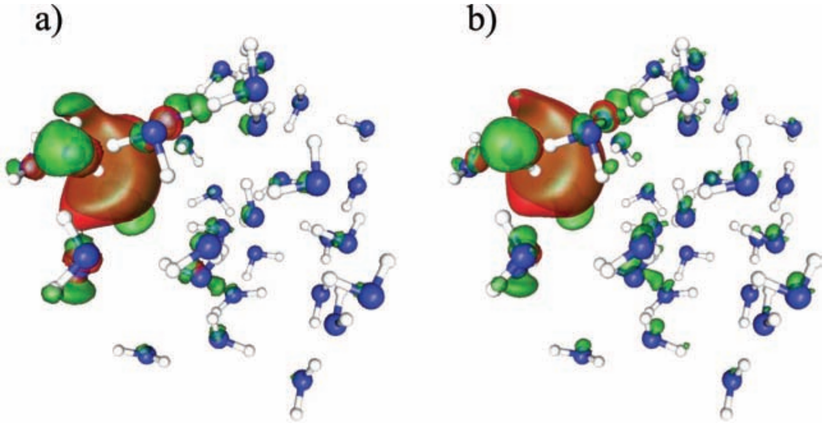

Figure 9. Spin density (red) and differential electronic density (green) at a 0.002 isovalue as computed at the (a) PBE-GTH-m-TZV2P and (b) RIMP2 levels. Note the almost perfect overlap between the spin and differential electronic densities for the main lobe and the slightly more diffuse character of the latter.

trajectory segment from $t = 3$ ps to $t = 9$ ps, characterized by a relatively stable surface-located excess electron. Several evenly symmetrized time series with a length of $t_{TOT}/2$ (where t_{TOT} is the total length of the 6-ps segment) were obtained by shifting the time origin by 125 fs along the simulated trajectory. For each time series, a discrete Fourier transform was performed in conjunction with application of a Blackman smoothing function.[64] The resulting spectrum shows three different bands (Figure 4), corresponding to libration and intramolecular bending and stretching modes. We focus here on the H−O−H bending region, where the AA signature is expected as a red-shifted side peak. Because the short duration of the simulation does not allow the two peaks, which are expected to be separated by about 100 cm^{-1},[20] to be distinguished, the IR spectrum was decomposed into three parts. The first part was obtained by restricting the computation of the velocity autocorrelation function to the water molecule closest to the electron center. Next, the second- through the sixth-closest molecules were considered, and the last spectrum was computed as a contribution from the remaining 26 H_2O molecules. In Figure 4, the three IR spectra are shown, focusing on the bending region. Although the spectra obtained from all molecules and from the 26 water molecules that are more distant from e_{aq}^- are quite similar to each other, the higher-frequency peak at 1250 cm^{-1} disappears when only the closest molecules are considered. The fact that, in contrast, the lower-frequency peak at around 1130 cm^{-1} persists even when only the closest water molecule to the excess electron indicates a possible occurrence of the AA motif.

Aside from vibrational spectra, a simple geometrical criterion can yield additional information about e_{aq}^- solvation structure. Specifically, we compared the average distance between the electron center and the two hydrogen atoms of the closest H_2O molecule to the excess electron with the same quantity averaged over the six closest molecules (Figure 5). This allowed us to identify geometries in which several water molecules interact similarly with the excess electron (in this case, the two curves show similar values) from AA-type structures. There, the approximate symmetry of the solvent shell is broken, and a single molecule is significantly closer to the excess electron than the others (therefore, the two curves deviate). From Figure 5, one can see that there are frequent interconversions between these two situations. Examining the excess electron density at $t = 6.12$ ps, corresponding to a large difference between the two averaged distances, a clear AA motif is seen, with one H_2O molecule located very close to the electron and pointing both hydrogen atoms toward the electronic cloud (Figure 6). In contrast, a situation in which the two curves in Figure 5 are close to each other, such as that at $t = 6.62$ ps, is characterized by several water molecules surrounding the excess electron, each donating a single hydrogen bond to it (Figure 7).

Comparison with Higher-Level ab Initio Calculations. The accuracy of the DFT level of theory underlying the dynamical calculations was tested against benchmark calculations for representative snapshots extracted from the simulated trajectory. The analysis was restricted to the trajectory segment from $t = 0$ ps to $t = 3$ ps, which covers all the important patterns investigated, that is, interior, delocalized, and surface-localized excess electrons. Single-point calculations at the PBE-GTH-m-TZV2P level with the self-interaction correction were computed at regular 300-fs intervals. B3LYP/6-31++G** and RIMP2/aug-cc-pVDZ calculations, which are rather costly, were performed for several snapshots representing an internally localized, an externally localized, and a delocalized excess electron.

Figure 8 summarizes the benchmarking results. First, note that the computed quantities are only weakly modified when the SIC term is included. The excess electron is somewhat more localized, and the VDE values are slightly higher when the self-interaction error is removed, whereas the electron position R_d is basically left unchanged. Interestingly, the SIC term was found to be more important in simulations of an excess electron on ice.[32] In ref 32, one illustration of the importance of the SIC is the calculation of the electron affinity (EA) of a single water molecule. The reported value for an uncorrected BLYP calculation is 1 eV, whereas the SIC calculation yields a vanishingly small EA, in agreement with experiment. The large EA obtained with a standard generalized gradient approximation (GGA) is a surprising result, which we tried to reproduce. Calculating the EA of a nearly unbound, and thus very diffuse, electron is not straightforward. Calculations based on Gaussian basis sets require very diffuse functions,[65] whereas plane-wave calculations require very large unit cells and proper boundary conditions (i.e., nonperiodic) for the electrostatic calculations. We note that the electron affinity computed using periodic boundary conditions depends on the conventional zero of the potential and that the SIC might change that convention. Here, we employed a cubic unit cell with 40-Å edges, nonperiodic boundary conditions, and a TZV2PX basis for oxygen augmented with 10 sets of diffuse s and p functions with common exponents ranging from 0.16 to 0.0003125 in a geometric progression. With this setup, we obtained an EA of less than 0.1 eV and suggest that this value will converge to ~0 eV (in agreement with experiment; calculations can actually still show a marginal binding of the electron due to the use of the Born–Oppenheimer approximation) for even larger unit cells. This result was obtained without the need to resort to an SIC.

The B3LYP results are also in very good agreement with values extracted from the MD simulations, with the observed transition from an internally localized to an externally localized electron taking place through the same delocalized electron state. There, the excess electron is slightly more delocalized and farther from the cluster center at the B3LYP level. Comparison with our most accurate RIMP2/aug-cc-pVDZ level of theory is revealing. In full agreement with the DFT results, the RIMP2 calculations yield an internally localized electron for the first snapshot considered and an externally localized electron for the last case, with both R_e and R_d values being well reproduced. Moreover, the VDEs at the RIMP2 level are in very good agreement with the PBE-GTH-m-TZV2P values. The transition from an internal to an external excess electron occurs through a delocalized state at the RIMP2 level, as well. However, as can be seen from the R_e and R_d values computed for intermediate configurations, a shorter delocalized phase is observed at the RIMP2 level, with the electron being pushed faster and farther from the cluster center than for all of the DFT calculations.

As a check of basis set convergence, we added additional diffuse functions centered at the atom closest to the electron center of mass (two sets of diffuse s and p functions sharing the same exponents of 0.015 and 0.003) for two selected geometries, one ($t = 1.2$ ps) corresponding to a very delocalized excess electron and the other ($t = 3$ ps) corresponding to a localized surface electron. In both cases, the change in binding energy was found to be small (<0.1 eV). Additionally, we verified the vanishing difference between the spin and differential electronic densities. This difference is very small both at RIMP2 and PBE-GTH-m-TZV2P levels. Figure 9 shows how the two densities coincide, with the differential density being slightly more diffuse.

In conclusion, the PBE-GTH-m-TZV2P method performs very well for the description of both interior and surface-localized excess electrons. However, it tends to overestimate the delocalization and time scale related to the bulk-to-surface transition of the excess electron.

Discussion. The present calculations provide data that can be related to various experimental observables. First, however, one should be aware that it is, in principle, possible that a more stable structure, characterized by an internally solvated electron, might exist that has a very different structure than $I^-(H_2O)_{32}$ and that the two structures are separated by a very large energy barrier, that cannot be overcome because of the limited length of our simulations. Nevertheless, previous theoretical and experimental research, summarized below, does not seem to support this hypothesis, confirming our findings.

A direct contact with experiments is obtained by comparing the VDEs with electron photodetachment spectra.[14,15] In Figure 2, two peaks are seen in our VDE distribution. This is superficially similar to a recent experimental result,[15] where the lower energy peak is assigned to a surface state and the second to a bulk state. However, the lack of correlation between the calculated VDEs and the excess electron position R_d (top panel in Figure 3) and the strong inverse relationship between the VDE and the electron radius of gyration (lower panel in Figure 3) lead us to a different interpretation of the spectrum. The lower VDE peak corresponds to a strongly delocalized e_{aq}^-, whereas the higher-energy peak reflects a localized excess electron. For most of our trajectory, the latter corresponds to a surface state; however, the initial internally localized electron state has a similar binding strength as the final surface state. Therefore, it also contributes (albeit marginally) to the higher-energy peak in the VDE spectrum. The bottom line is that the value of the VDE characterizes the degree of localization of the excess electron rather than its position within the cluster.

A second contact to experimental observables is through the IR spectrum. Note, however, that deuterated water was used in the simulations, which explains the shift between the simulated and measured vibrational peaks. It was recently observed that the AA motif of a single strongly interacting water molecule, characterized by a red-shifted peak in the bending region, is observed even for relatively large cluster.[20] As the cluster size increases further, this peak merges with the signal from water molecules that are not interacting as strongly with the excess electron. By decomposing the calculated IR spectrum into contributions from molecules at different distances from e_{aq}^- and using a simple geometrical criterion, it was possible to deduce that dynamical interconversions between AA and cavity structures occur. Such structures were also clearly recognized from the excess electron density plots.

Regarding comparison with other theoretical calculations, two previous studies concluded that, for clusters of the present size, electron surface solvation is favored over internal solvation.[17,21] This is in agreement with the present results. Quantitatively, compared to these one-electron pseudopotential calculations,[17] where a large average electron radius, R_{av}, was observed for the surface state (for $n = 30$, R_{av} was larger than 4 Å), our estimate of $R_{av} = 3.23$ Å is smaller and thus closer to the value for a bulk hydrated electron.

Conclusions

We performed a 15-ps ab initio MD simulation of a $(H_2O)_{32}^-$ cluster. By construction, the excess electron was initially located in the cluster interior. However, during the dynamics, the electron moved rapidly to the cluster surface within a ~2-ps transient phase characterized by a delocalized state. The electron then remained at the cluster surface for the rest of the simulated trajectory, with its radius of gyration being only slightly larger than its equilibrium bulk value most of the time. Therefore, we can confirm that, for water clusters of the size examined here, surface solvation is favored by the excess electron over an internal state. For interpretation of photoelectron spectra, it is important to note that the calculated VDE values did not show a correlation with the electron position within the cluster; however, a very strong correlation was found between the electron radius of gyration and the binding energy. A geometrical analysis of the solvation shell of the excess electron showed that two structures frequently interconvert. The first has several water molecules interacting in a similar fashion with the electron, whereas in the second, a single water molecule moves closer to the electronic cloud.[9,10] The computed IR spectrum, decomposed into contributions from different water molecules, confirmed this finding, as well as the repeated temporal presence of the AA binding motif of a single strongly bound water molecule.[20] Finally, we note that the PBE level of the DFT theory used for the MD electronic structure calculations compared well with benchmark calculations. In particular, it was found that the VDE values along the trajectory were in very good agreement with accurate RIMP2 predictions. When the electron was localized at the surface (or initially in the interior), the excess electron size and location were also accurately reproduced. Only in the transient phase, characterized by a very delocalized excess electron, was the degree of delocalization overestimated for all of the DFT methods employed.

Acknowledgment. P.J. acknowledges support from the Czech Ministry of Education (Grant LC 512) and the Granting Agency of the Czech Republic (Grant 202/06/0286). Some of the presented calculations were performed on the HLRN supercomputer. We thank Dr. Knut Asmis for very interesting discussions.

References and Notes

(1) *Excess Electrons in Dielectric Media*; Ferradini, C., Jay-Gerin, J.-P., Eds.; CRC Press: Boca Raton, FL, 1991.

(2) Lu, Q. B.; Sanche, L. *Phys. Rev. Lett.* **2001**, *87*, 078501.

(3) Lu, Q. B.; Sanche, L. *Phys. Rev. B* **2001**, *63*, 153403.

(4) Hart, E. J.; Boag, J. W. *J. Am. Chem. Soc.* **1962**, *84*, 4090.

(5) Tsurusawa, T.; Iwata, S. *Chem. Phys. Lett.* **1998**, *287*, 553.

(6) Tachikawa, H. *J. Chem. Phys.* **2006**, *125*, 144307.

(7) Clary, D. C.; Benoit, D. M. *J. Chem. Phys.* **1999**, *111*, 10559.

(8) Smith, D. M. A.; Smets, J.; Elkadi, Y.; Adamowicz, L. *J. Chem. Phys.* **1998**, *109*, 1238.

(9) Herbert, J. M.; Head-Gordon, M. *J. Am. Chem. Soc.* **2006**, *128*, 13932.

(10) Riscioli, J. R.; Hammer, N. I.; Johnson, M. A. *J. Phys. Chem. A* **2006**, *110*, 7517.

(11) Sommerfeld, T.; Jordan, K. D. *J. Phys. Chem. A* **2006**, *109*, 11531.

(12) Wang, F.; Jordan, K. D. *J. Chem. Phys.* **2002**, *116*, 6973.

(13) Sommerfeld, T.; Gardner, S. D.; DeFusco, A.; Jordan, K. D. *J. Chem. Phys.* **2007**, *125*, 174301.

(14) Coe, J. V.; Lee, G. H.; Eaton, J. G.; Arnold, S. T.; Sarkas, H. W.; Bowen, K. H.; Ludewigt, C.; Haberland, H.; Worsnop, D. R. *J. Chem. Phys.* **1990**, *92*, 3980.

(15) Verlet, J. R. R.; Bragg, A. E.; Kammrath, A.; Cheshnovsky, O.; Neumark, D. M. *Science* **2005**, *307*, 93.

(16) Coe, J. V.; Arnold, S. T.; Eaton, J. G.; Lee, G. H.; Bowen, K. H. *J. Chem. Phys.* **2006**, *125*, 014315.

(17) Turi, L.; Sheu, W. S.; Rossky, P. J. *Science* **2005**, *309*, 914.

(18) Turi, L.; Madarasz, A.; Rossky, P. J. *J. Chem. Phys.* **2006**, *125*, 014308.

(19) Khan, A. *J. Chem. Phys.* **2006**, *125*, 024307.

(20) Asmis, K. R.; Santambrogio, G.; Zhou, J.; Garand, E.; Headrick, J.; Goebbert, D.; Johnson, M. A.; Neumark, D. M. *J. Chem. Phys.* **2007**, *126*, 191105.

(21) Barnett, R. N.; Landman, U.; Cleveland, C. L.; Jortner, J. *J. Chem. Phys.* **1988**, *88*, 4429.

(22) Makov, G.; Nitzan, A. *J. Phys. Chem.* **1994**, *98*, 3459.

(23) Tauber, M. J.; Mathies, R. A. *J. Am. Chem. Soc.* **2003**, *125*, 1394.

(24) Rossky, P. J.; Schnitker, J. *J. Phys. Chem.* **1988**, *92*, 4277.

(25) Schnitker, J.; Motakabbir, K.; Rossky, P. J.; Friesner, R. *Phys. Rev. Lett.* **1988**, *60*, 456.

(26) Skorobogatiy, M.; Park, I. J.; Joannopolous, J. D. *Comput. Mater. Sci.* **2005**, *32*, 96.

(27) Boutin, A.; Spezia, R.; Coudert, F.; Mostafavi, M. *Chem. Phys. Lett.* **2005**, *409*, 219.

(28) Turi, L.; Borgis, D. *J. Chem. Phys.* **2002**, *117*, 6186.

(29) Boero, M.; Parrinello, M.; Terakura, K.; Ikeshoji, T.; Liew, C. C. *Phys. Rev. Lett.* **2003**, *90*, 226403.

(30) Boero, M. *J. Phys. Chem. A* **2007**, *111*, 12248.

(31) Shkrob, I. A.; Glover, W. J.; Larsen, R. E.; Schwartz, B. J. *J. Phys. Chem. A* **2007**, *111*, 5232.

(32) Baletto, F.; Cavazzoni, C.; Scandolo, S. *Phys. Rev. Lett.* **2005**, *95*, 176801.

(33) Shkrob, I. A. *J. Phys. Chem. A* **2007**, *111*, 5223.

(34) Herbert, J. M.; Johnson, M. A. *Proc. Natl. Acad. Sci. U.S.A.* **2006**, *103*, 14282.

(35) CP2K Developers Group home page, http://cp2k.berlios.de, 2004.

(36) VandeVondele, J.; Krack, J.; Mohammed, F.; Parrinello, M.; Chassaing, T.; Hütter, J. *Comput. Phys. Commun.* **2005**, *167*, 103.

(37) Kuo, I. W.; Mundy, C. J.; McGrath, M. J.; Siepmann, J. I.; VandeVondele, J.; Hutter, J.; Sprik, M.; Hutter, J.; Chen, B.; Klein, M.; Mohammed, F.; Krack, M.; Parrinello, M. *J. Phys. Chem. B* **2004**, *108*, 12990.

(38) Goedecker, S.; Teter, M.; Hutter, J. *Phys. Rev. B* **1996**, *54*, 1703.

(39) Perdew, J. P.; Burke, K.; Ernzerhof, M. *Phys. Rev. Lett.* **1996**, *77*, 3865.

(40) VandeVondele, J.; Mohammed, F.; Krack, M.; Hütter, J.; Sprik, M.; Parrinello, M. *J. Chem. Phys.* **2005**, *122*, 014515.

(41) McGrath, M. J.; Siepmann, J. I.; Kuo, I. F. W.; Mundy, C. J. *Mol. Phys.* **2006**, *104*, 3619.

(42) VandeVondele, J.; Hutter, J. *J. Chem. Phys.* **2007**, *127*, 114105.

(43) Martyna, G.; Tuckermann, M. *J. Chem. Phys.* **1999**, *100*, 2810.

(44) Schwegler, E.; Grossman, J. C.; Gygi, F.; Galli, G. *J. Chem. Phys.* **2004**, *121*, 5400.

(45) Gräfenstein, J.; Kraka, E.; Cremer, D. *Phys. Chem. Chem. Phys.* **2004**, *6*, 1096.

(46) VandeVondele, J.; Sprik, M. *Phys. Chem. Chem. Phys.* **2005**, *7*, 1363.

(47) Becke, A. D. *J. Phys. Chem.* **1993**, *98*, 5648.

(48) Lee, C.; Yang, W.; Parr, R. G. *Phys. Rev. B* **1988**, *37*, 785.

(49) Hehre, W. J.; Ditchfield, R.; Pople, J. A. *J. Chem. Phys.* **1972**, *56*, 2257.

(50) Weigend, F.; Haeser, M. *Theor. Chem. Acc.* **1997**, *97*, 331.

(51) Weigend, F.; Haeser, M.; Patzelt, H.; Ahlrichs, R. *Chem. Phys. Lett.* **1998**, *294*, 143.

(52) Kendall, R. A.; Dunning, T. H.; Harrison, R. J. *J. Chem. Phys.* **1992**, *96*, 6796.

(53) Herbert, J. M.; Head-Gordon, M. *J. Phys. Chem. A* **2005**, *109*, 5217.

(54) Frisch, M. J.; Trucks, G. W.; Schlegel, H. B.; Scuseria, G. E.; Robb, M. A.; Cheeseman, J. R.; Montgomery, J. A., Jr.; Vreven, T.; Kudin, K. N.; Burant, J. C.; Millam, J. M.; Iyengar, S. S.; Tomasi, J.; Barone, V.; Mennucci, B.; Cossi, M.; Scalmani, G.; Rega, N.; Petersson, G. A.; Nakatsuji, H.; Hada, M.; Ehara, M.; Toyota, K.; Fukuda, R.; Hasegawa, J.; Ishida, M.; Nakajima, T.; Honda, Y.; Kitao, O.; Nakai, H.; Klene, M.; Li, X.; Knox, J. E.; Hratchian, H. P.; Cross, J. B.; Bakken, V.; Adamo, C.; Jaramillo, J.; Gomperts, R.; Stratmann, R. E.; Yazyev, O.; Austin, A. J.; Cammi, R.; Pomelli, C.; Ochterski, J. W.; Ayala, P. Y.; Morokuma, K.; Voth, G. A.; Salvador, P.; Dannenberg, J. J.; Zakrzewski, V. G.; Dapprich, S.; Daniels, A. D.; Strain, M. C.; Farkas, O.; Malick, D. K.; Rabuck, A. D.; Raghavachari, K.; Foresman, J. B.; Ortiz, J. V.; Cui, Q.; Baboul, A. G.; Clifford, S.; Cioslowski, J.; Stefanov, B. B.; Liu, G.; Liashenko, A.; Piskorz, P.; Komaromi, I.; Martin, R. L.; Fox, D. J.; Keith, T.; Al-Laham, M. A.; Peng, C. Y.; Nanayakkara, A.; Challacombe, M.; Gill, P. M. W.; Johnson, B.; Chen, W.; Wong, M. W.; Gonzalez, C.; and Pople, J. A. *Gaussian 03*, revision C.02; Gaussian, Inc.: Wallingford, CT, 2004.

(55) Ahlrichs, R.; Bär, M.; Häser, M.; Horn, H.; Kölmel, C. *Chem. Phys. Lett.* **1989**, *162*, 165.

(56) (a) Straatsma, T. P.; Aprà, E.; Windus, T. L.; Bylaska, E. J.; de Jong, W.; Hirata, S.; Valiev, M.; Hackler, M.; Pollack, L.; Harrison, R.; Dupuis, M.; Smith, D. M. A.; Nieplocha, J.; Tipparaju V.; Krishnan, M.; Auer, A. A.; Brown, E.; Cisneros, G.; Fann, G.; Früchtl, H.; Garza, J.; Hirao, K.; Kendall, R.; Nichols, J.; Tsemekhman, K.; Wolinski, K.; Anchell, J.; Bernholdt, D.; Borowski, P.; Clark, T.; Clerc, D.; Dachsel, H.; Deegan, M.; Dyall, K.; Elwood, D.; Glendening, E.; Gutowski, M.; Hess, A.; Jaffe, J.; Johnson, B.; Ju, J.; Kobayashi, R.; Kutteh, R.; Lin, Z.; Littlefield, R.; Long, X.; Meng, B.; Nakajima, T.; Niu, S.; Rosing, M.; Sandrone, G.; Stave, M.; Taylor, H.; Thomas, G.; van Lenthe, J.; Wong, A.; Zhang, Z. *NWChem: A Computational Chemistry Package for Parallel Computers*, version 4.6; Pacific Northwest National Laboratory: Richland, WA, 2004. (b) Kendall, R. A.; Aprà, E.; Bernholdt, D. E.; Bylaska, E. J.; Dupuis, M.; Fann, G. I.; Harrison, R. J.; Ju, J.; Nichols, J. A.; Nieplocha, J.; Straatsma, T. P.; Windus, T. L.; Wong, A. T. *Comput. Phys. Commun.* **2000**, *128*, 260.

(57) Humphrey, W.; Dalke, A.; Schulten, K. *J. Mol. Graphics* **1996**, *14*, 33.

(58) Laaksonen, L. *J. Mol. Graphics* **1992**, *10*, 33.

(59) Bergman, D. L.; Laaksonen, L.; Laaksonen A, *J. Mol. Graphics Modell.* **1997**, *15*, 301.

(60) Cornell, W. D.; Cieplak, P.; Bayly, C. I.; Gould, I. R.; Merz, K. M.; Ferguson, D. M.; Spellmeyer, D. C.; Fox, T.; Caldwell, J. W.; Kollman, P. A. *J. Am. Chem. Soc.* **1996**, *118*, 2309.

(61) Tuttle, T. R.; Golden, S. J. *J. Phys. Chem.* **1991**, *95*, 5725.

(62) Jou, F.-Y.; Freeman, G. R. *J. Phys. Chem.* **1979**, *83*, 2383.

(63) Jungwirth, P.; Tobias, D. J. *J. Phys. Chem. B* **2002**, *106*, 6361.

(64) Harris, F. J. *Proc. IEEE* **1978**, *66*, 51.

(65) Chipman, D. M. *J. Phys. Chem.* **1978**, *82*, 1080.

JP711545S